

# High Efficiency Integrated Transformer Design in DAB Converters for Solid-State Transformers

Eun S. Lee<sup>✉</sup>, Member, IEEE, Jin H. Park, Member, IEEE, Myung Y. Kim<sup>✉</sup>, Member, IEEE,  
and June S. Lee<sup>✉</sup>, Member, IEEE

**Abstract**—Solid-state transformers (SST) are emerging technologies to replace the conventional low-frequency main transformer (MTr) in railway vehicles. In order to isolate the load side from the AC 25 kV high-voltage (HV) side and to reduce the whole size of the SST, HV insulation and high-frequency transformers should be used in DC/DC converters. Furthermore, due to the severe constraint of installation space and difficulty of heat dissipation management in the bottom of railway vehicles, high-power density and minimum transformer loss should be considered. To satisfy such design requirements of the proposed SST for railway vehicles, high efficiency integrated transformers, which inherently have leakage inductance, are proposed for dual-active-bridge (DAB) converters in this paper. In order to obtain appropriate equivalent leakage inductance for the DAB converters, a calculation methodology for the leakage inductance has been introduced and verified by simulation. Two separated winding structures in the center-core are adopted to improve the core loss, and appropriate winding turns with 60 kV HV insulation capability are selected, according to the proposed design procedure of the integrated transformers. In order to compare the proposed transformers with the conventional transformer having additional inductors and to verify the major characteristics of the transformers, two 125 kW proposed transformers and conventional transformers have been built and evaluated by an 250 kW SST module, operating at 10 kHz switching frequency. Under a 125 kW full-load condition, 99.7% transformer efficiency was obtained by the proposed integrated transformers, which are 4.7% smaller and 7.0% lighter than the conventional transformer. As a result, 26°C maximum temperature improvement has been obtained and 60kV HV insulation capability has been satisfied by the proposed integrated transformers.

**Index Terms**—Solid-state transformer (SST), railway vehicles, integrated transformers, high-voltage insulation, dual-active-bridge.

## I. INTRODUCTION

RAILWAY vehicles are fast and convenient means to transport passengers as public transportation and freight. They

Manuscript received October 10, 2021; revised January 16, 2022 and March 6, 2022; accepted April 8, 2022. Date of publication April 19, 2022; date of current version July 18, 2022. This work was supported by the Railroad Technology Development Program funded by the Ministry of Land, Infrastructure and Transport (MOLIT) of Korean Government under Grant 21RSCD-C163337-01. The review of this article was coordinated by Dr. Mehdi Narimani. (*Corresponding author: Eun S. Lee*.)

Eun S. Lee is with the Division of Electrical Engineering, Hanyang University ERICA, Ansan 15588, South Korea (e-mail: eunsoo86@hanyang.ac.kr).

Jin H. Park and Myung Y. Kim are with the Propulsion System Research Team, Korea Railroad Research Institute (KRRI), Uiwang 16105, South Korea (e-mail: powerword@krri.re.kr; mykim@krri.re.kr).

June S. Lee is with the Department of Electrical Engineering, Dankook University, Yongin 31116, South Korea (e-mail: ljs@dankook.ac.kr).

Digital Object Identifier 10.1109/TVT.2022.3168561

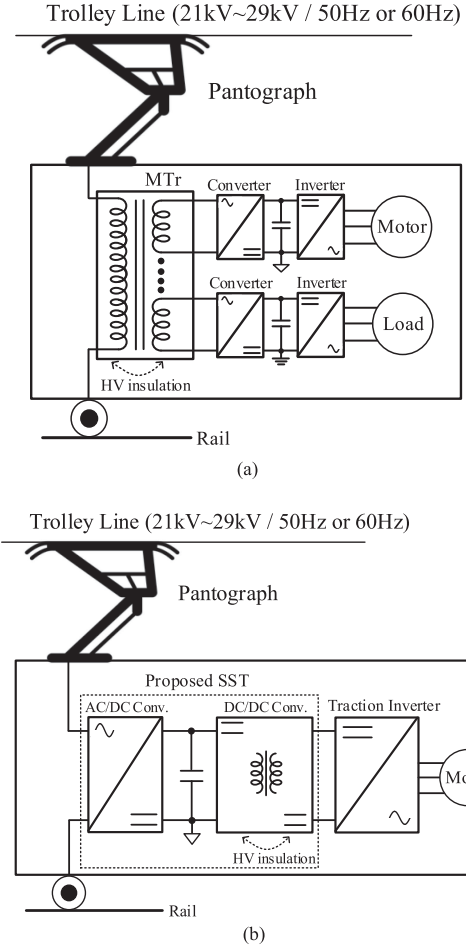


Fig. 1. Conventional and proposed concepts of the power conversion systems. (a) Conventional power conversion systems, including MTr. (b) Proposed SST.

can be operated by trolley lines, which provide several tens of kilo voltage having large power transmission capability. It is thus important to design high efficiency power conversion systems in railway vehicles, converting the high-voltage (HV) AC source to a low-voltage (LV) DC source [1]–[8]. As the first stage of the power conversion system in railway vehicles, 50 Hz or 60 Hz main transformers (MTr) are conventionally used, as shown in Fig. 1(a). In this case, AC/DC converters are used to provide traction inverters with LV DC sources. Due to the low operating frequency of the MTr, the power conversion systems are inevitably bulky, and inconvenient for maintenance.

Furthermore, in the case of a defective situation of the MTr, the power conversion systems will no longer provide power with traction motors and various loads; highly reliable and compact power conversion systems are hence necessary due to the low reliability and large size of the conventional MTr. For these reasons, a solid-state transformer (SST) is a promising solution to replace the conventional MTr, as shown in Fig. 1(b). The principle of the SST technologies is basically to use high switching frequency in isolated DC/DC converter stages so that the size of isolated transformers in the SST can be reduced. Because the SST system adopts plenty of modules, reliable operation is possible by using a bypass mode of the corresponding failed module, even when one of SST modules is in a failure situation [1]–[5].

There are many possible SST topologies in terms of AC/AC converters, AC/DC converters and DC/DC converters w.r.t. the power and voltage levels, the number of modules, switching frequency, and control methods [1]–[8]. The prime goal of the SST developments is not only to realize active power control from HV to LV sides, but also to reduce the size and weight of the power conversion systems. Railway vehicles involve the most challenging conditions for SST applications due to limited installation space of the power conversion system [1]–[4]. If the switching frequency in DC/DC converters increases to reduce the size of the isolated transformers, the power loss in the switching devices rises, which results in a large heat-sink and low power efficiency. Therefore, if the switching frequency no longer increases or decreases due to the inherent characteristics of the switching devices and heat dissipation management, the isolated transformers in DC/DC converters should be minimized as much as possible.

When selecting an appropriate topology of the DC/DC converters for SSTs, dual-active-bridge (DAB) converters are widely used as an isolation-type bidirectional DC/DC converter due to the use of fewer components, a simple circuit structure, low switching losses, bidirectional power flow capability, low sensitivity to parasitic components, and a relatively wide-range of zero-voltage switching (ZVS) operations [1]–[4], [8]–[10]. In order to isolate the HV side from the LV side and to utilize the magnetic energy storage components, high-frequency transformers and additional inductors are used in the DAB converters. Using additional inductors, however, increases the total volume and weight of the DAB converters.

Several attempts to remove additional inductors by using inherent leakage inductance for the DAB converters have been reported [11]–[14]. Although the leakage inductance can be obtained by modulating the center-core airgap [11], the gap between primary and secondary windings wound in the center core [12]–[13], and the number of windings turns [14], the equivalent leakage inductance cannot be exactly found due to the non-specified magnetic leakage path. Thus, numerous iterative processes should be implemented under various variables, e.g., core airgap, winding airgap, and winding turns; finding the appropriate leakage inductance is accordingly very time consuming [11]–[14]. There are other previous research to obtain the leakage integration into one transformer by special transformer structures [15]–[16] and inserting additional magnetic

materials into the transformer cores [17]–[19]. Improved planar structure-based transformers can be used and they include designated legs with flux paths to obtain leakage inductance [15]–[16]. In addition, intentional airgap between primary and secondary windings were adopted to obtain appropriate leakage inductance [17]. However, these transformer structures are so complicated and require high cost to be manufactured [15]–[17]. Furthermore, the maximum allowable leakage inductance is limited by the physical maximum height of airgap between the primary and secondary windings. To overcome this limitation of the maximum allowable leakage inductance in airgap, magnetic shunt is applied into airgap between the primary and secondary windings [18]–[19]. However, this additional magnetic shunt has major demerits: manufacture complexity, high assembly cost, additional core loss in the magnetic shunt, and temperature-dependent permeability, leading to unsettled leakage inductance. Furthermore, those previous research do not consider the high voltage insulation capability, which is essential for high power applications. Therefore, a simple but useful methodology to obtain high leakage inductance with high voltage insulation is required.

In order to theoretically specify the equivalent leakage inductance for DAB converters, high-efficiency operation and HV insulation integrated transformers targeting railway vehicle SST applications are proposed in this paper. To obtain the appropriate equivalent leakage inductance, a calculation methodology for deriving the leakage inductance in the transformers is introduced for the optimally designed transformer having minimum transformer loss. Furthermore, in order to reduce the core loss and to guarantee the HV insulation capability, two separated coil winding structures are applied. Thus, high-power density and thermal-stable operation are possible by selecting an appropriate number of windings turns in the proposed integrated transformers. A 250 kW SST module has been fabricated and utilized to verify the proposed and conventional transformers, showing that the proposed transformer is superior to the conventional transformer in terms of weight, volume, thermal management, and HV insulation capability.

## II. DESIGN REQUIREMENT OF THE PROPOSED INTEGRATED TRANSFORMERS FOR SST

The proposed SST consists of two stages: cascaded H-bridge (CHB) based AC/DC converters and DAB converters for isolated DC/DC converters, as shown in Fig. 1(b). In order to divide large grid voltage (= trolley line voltage) of 25 kV, multi-level CHB converters are used, and the DC-link voltages are connected to the DAB converters in this study [1]. Because the grid voltage is 25 kV, and load voltage is 1.5 kV for urban railway vehicles, the input-series and output-parallel (ISOP) modular configuration is adopted to decrease the voltage level, as shown in Fig. 2. A bypass switch  $S_b$  is used to bypass the fault detected module. In one CHB converter, two DAB converters are used in series due to the inherent voltage stress of the switching devices. In the HV and LV stacks, half-bridge and full-bridge converters are used, respectively, to decrease the voltage level. In the conventional

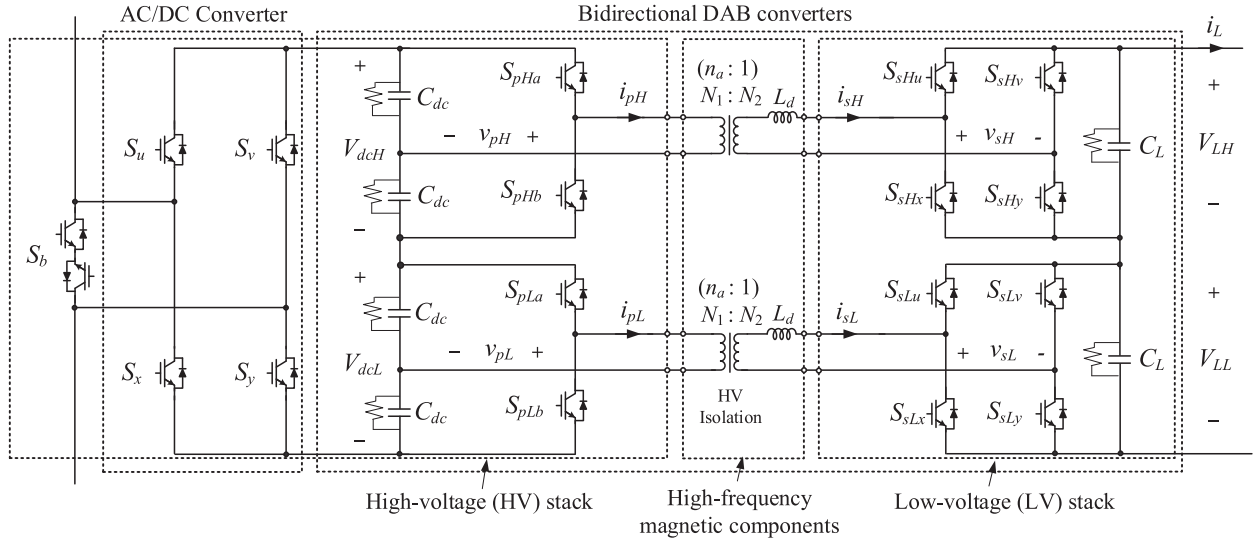


Fig. 2. Circuit configuration of one module for the SST.

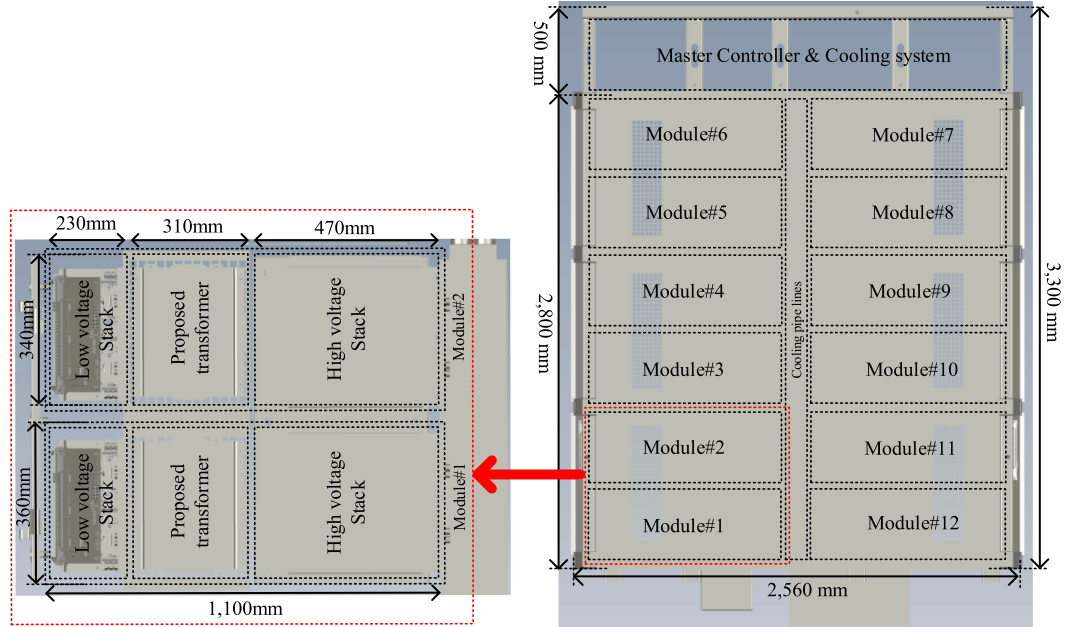


Fig. 3. Component arrangements and the size information for the proposed SST.

DAB converters, high-frequency magnetic components including isolation transformers and additional inductors should be used.

In order to reduce the voltage level from the input to the output side,  $N_1$  is larger than  $N_2$  in the isolation transformers. It is important to guarantee HV insulation between the primary and secondary sides through the high-frequency transformer. The switching frequency of the DAB converters is selected as 10 kHz, considering the total switching and conduction losses for the switching devices, as well as the total volume of the magnetic components [1]. The size of HV and LV stacks can be determined from the size information of switching devices, heat-sink, and capacitors, as shown in Fig. 3. Total size of the proposed SST is already determined, considering the possible installation space

in the bottom of the urban railway vehicles. Because the optimal number of SST modules can be selected in terms of total cost, complexity, and power loss, it is assumed that 12 modules are used in this railway vehicle SST applications [1]. From these SST design criteria, the maximum allowable installation space for the magnetic components is only 340 mm × 310 mm × 690 mm. Because the total maximum power is 3.0 MW for this application, one SST module occupies 250 kW, and the power transfer capability of the transformer is 125 kW in this paper.

To specify the design requirements of the proposed integrated transformers, operating conditions for the DAB converters should be determined. By using simple phase-shift control between primary and secondary sides, the DAB delivery power  $P_L$  and the primary and secondary currents  $i_p$  and  $i_s$  can be found

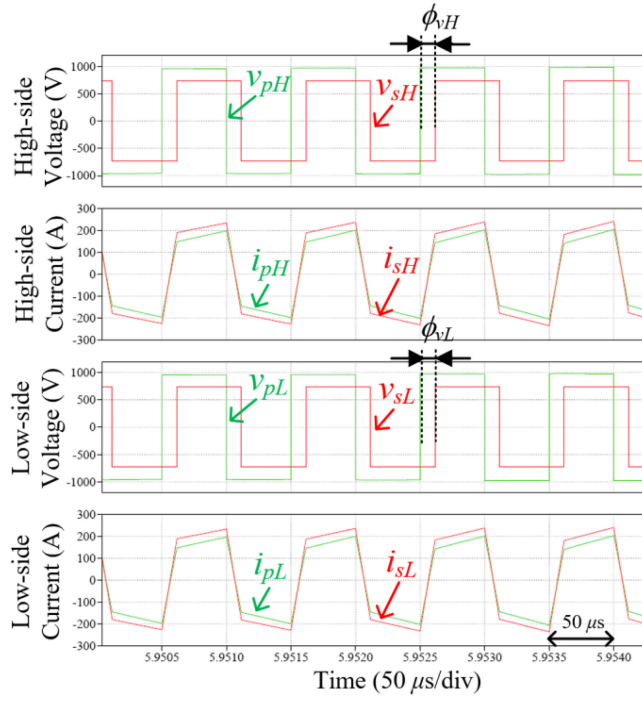


Fig. 4. Simulation waveforms for the DAB converter when the module power ( $=2P_L$ ) is 250 kW.

as follows [1]–[3], [8]–[10]:

$$P_L = \frac{2}{T_s} \int_0^{\frac{T_s}{2}} v_s(t) \cdot i_s(t) dt = \frac{V_p V_s \varphi_v (\pi - \varphi_v)}{2n_a \pi^2 L_d f_s} \quad (1a)$$

$(\because 0 < \varphi_v \leq \pi)$

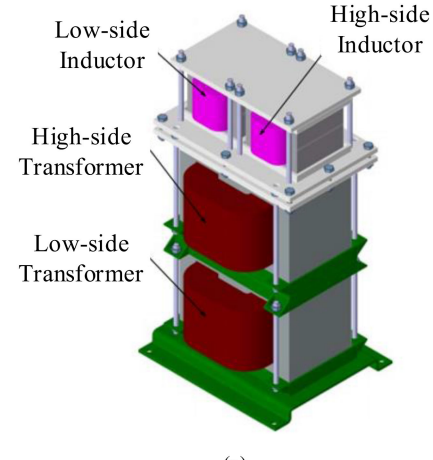
$$I_p = \sqrt{\frac{1}{T_s} \int_0^{T_s} i_p^2(t) dt}, \quad I_s = \sqrt{\frac{1}{T_s} \int_0^{T_s} i_s^2(t) dt} \quad (1b)$$

where  $n_a$  ( $= N_1/N_2$ ) is the turn ratio of the isolation transformer. It is noted that the primary and secondary currents  $i_p(t)$  and  $i_s(t)$  can be straightforwardly calculated w.r.t. the switching modes of the primary and secondary sides in the time domain [11].

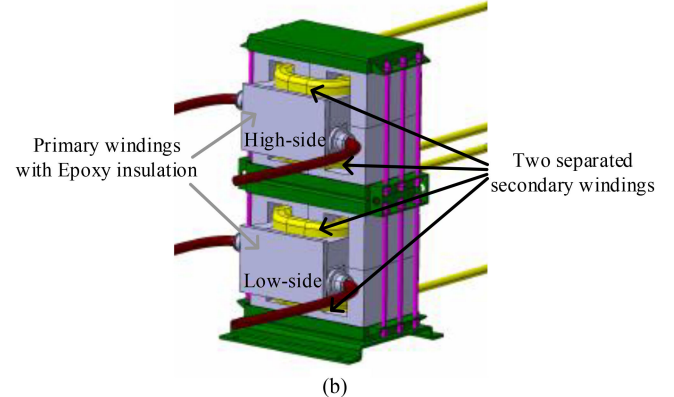
Because it is assumed that the DC-link voltage ( $V_{dc} = V_{dcH} + V_{dcL}$ ) is regulated to be 4.0 kV by the CHB converters for the 12-modules condition, the primary voltage  $V_p$  is calculated as 1.0 kV. Due to  $V_L (= V_{LH} + V_{LL}) = 1.5$  kV, the secondary voltage  $V_s$  is 750 V. It is assumed that the phase difference between the primary and secondary voltages  $\phi_v$  in (1a) is normally operated at nearly  $45^\circ$  for maximum load power delivery, considering the linear control slope of the DAB converters [1]–[4], and the turn ratio  $n_a$  is  $1.3 \sim 1.5$ , considering the flexible transformer design process. The required equivalent inductance  $L_d$  in Fig. 2 can then be calculated as  $35.0 \mu\text{H}$  from (1a). Based on these design results of the DAB converters, simulation waveforms for  $P_L = 125$  kW are shown in Fig. 4. As capacitor voltage balancing controls, DC-link voltage  $V_{dc}$  balancing control for all modules and two DC-link voltages balancing control between  $V_{dcH}$  and  $V_{dcL}$  in each module are applied in this paper [1]. By virtue of the voltage balancing control, the primary and secondary capacitor voltages are well balanced for high-side and low-side DAB converters, as

TABLE I  
PARAMETER SELECTIONS OF THE DAB CONVERTERS FOR THE PROPOSED SST

Parameters	Values	Parameters	Values
$V_p$	1.0 kV	$n_a$	$1.3 \sim 1.5$
$V_s$	750 V	$f_s$	10 kHz
$\phi_v$	$42^\circ \sim 60^\circ$	$L_d$	$35.0 \mu\text{H}$



(a)



(b)

Fig. 5. Overall structures of the magnetic components for DAB converters. (a) Conventional transformers with inductors. (b) Proposed integrated transformers having inherent leakage inductance.

shown in Fig. 4. The parameter selections for the DAB converters are summarized in Table I, and the same values will be used for simulation and experimental verifications.

### III. DESIGN METHODOLOGY OF THE PROPOSED INTEGRATED TRANSFORMERS

#### A. Comparison of Conventional and Proposed Transformers

The conventional magnetic components in Fig. 1 are usually composed of high-frequency transformers and additional inductors, as shown in Fig. 5(a) [1]–[4], [8]–[10]. Because two DAB converters are used in one module, two transformers and two inductors should be used, and their magnetic component sets are bulky and heavy for the limited installation space. On the other hand, only two transformers can be used in the proposed

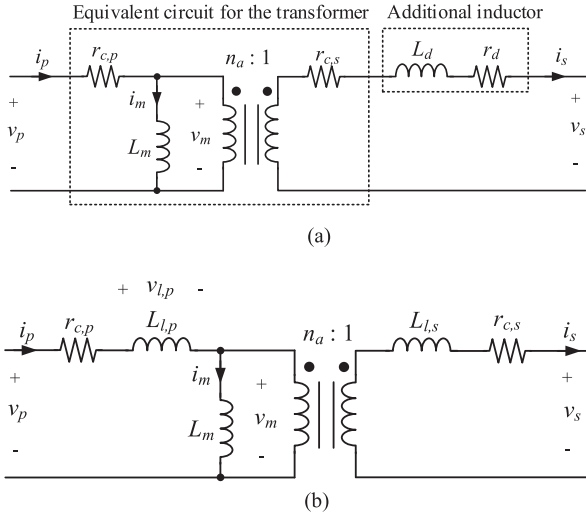


Fig. 6. Equivalent circuits of the magnetic components. (a) Conventional one. (b) Proposed one.

integrated transformers, as shown in Fig. 5(b). Primary windings are packaged by epoxy insulation to enhance the HV insulation capability, and two separated secondary windings are used to improve core loss in this paper. The equivalent circuits of Fig. 5 for the conventional and proposed transformers are shown in Fig. 6.  $r_{c,p}$  and  $r_{c,s}$  are the copper loss resistance for primary and secondary windings, and  $L_m$  is the magnetizing inductance. In order to design the proposed integrated transformers, an equivalent leakage inductance should be equal to the additional inductance as follows:

$$L_d = L_{l,p}/n_a^2 + L_{l,s} \quad (2)$$

The operating waveforms of the proposed integrated transformer for  $V_p > n_a V_s$  are described in Fig. 7. Then, the magnetizing current  $i_m$  can be expressed, assuming that the voltage drop caused by  $r_{c,p}$  is neglected for simplicity of analysis due to  $V_p \gg I_p \times r_{c,p}$  in this paper, as follows:

$$i_m(t) = \frac{v_m(t)}{\omega_s L_m} \approx \frac{v_p(t) - v_{l,p}(t)}{\omega_s L_m} \quad (3)$$

From (3), the magnetic field inside the ferrite core  $B_c$  can be calculated by the primary winding turns  $N_p$ , assuming that the leakage magnetic field is extremely smaller than magnetizing magnetic field ( $L_m \gg L_{l,p}$ ), as follows:

$$B_c(t) = \frac{v_m(t)}{\omega_s N_p A_c} \quad (4)$$

Based on the calculation results of (4), the primary winding turns  $N_p$  has the minimum design standard if the physical dimensions of the transformer are decided, satisfying that  $B_c$  is below the magnetic saturation level of the ferrite core  $B_{sat}$  at the maximum magnetizing current point  $i_m(t_2)$  in Fig. 7, as follows:

$$|B_c| < B_{sat} \approx 0.3T \\ \rightarrow \therefore N_p > \frac{v_m(t_2)}{\omega_s B_{sat} A_c} \approx \frac{n_a^2 L_{l,s} V_p + n_a L_{l,p} V_s}{1.88 f_s A_c (L_{l,p} + n_a^2 L_{l,s})} \quad (5)$$

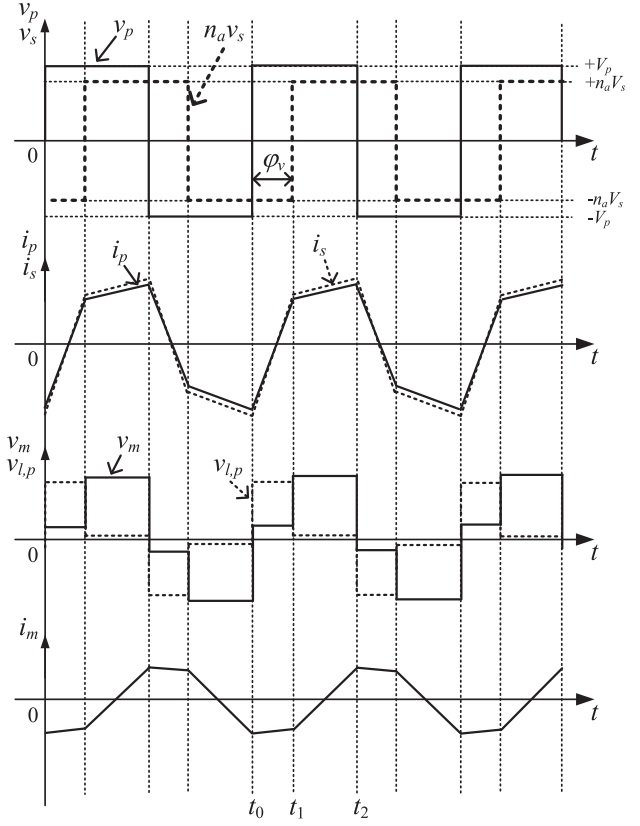


Fig. 7. Operating waveforms of the proposed integrated transformers in DAB converters ( $V_p > n_a V_s$ ).

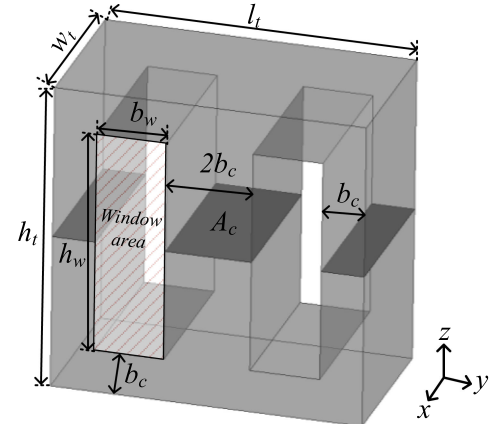


Fig. 8. Geometrical core structure of the proposed integrated transformers.

where  $A_c$  is the magnetic path area in the proposed transformers.

#### B. Leakage Inductance Calculation

In order to specify the equivalent leakage inductance, the geometrical structure of the proposed integrated transformers is shown in Fig. 8. The total size of the proposed transformer is  $l_t = 290$  mm,  $w_t = 160$  mm and  $h_t = 290$  mm in this paper, considering the allowable installation space for the proposed transformers in Fig. 3. Primary and secondary windings are wound in the center-core within the window area, as described

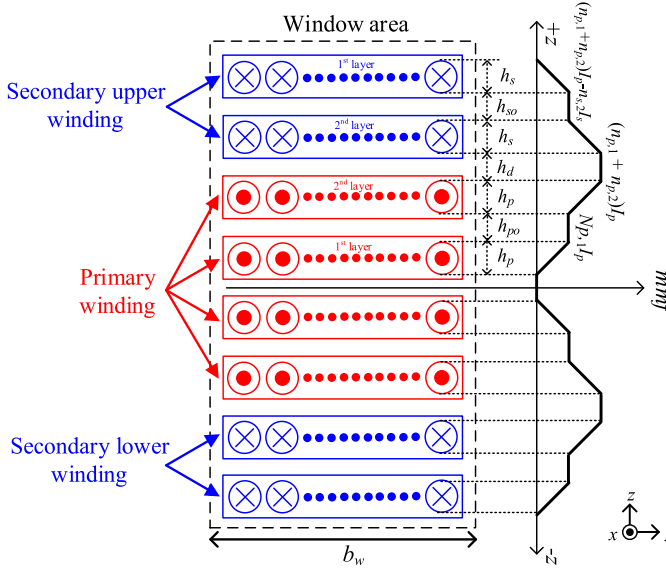


Fig. 9. Simplified theoretical configuration of mmf distribution w.r.t. winding positions.

in Fig. 5(b). The effective length of the magnetic field path  $l_e$  and magnetic path area  $A_c$  can then be defined from Fig. 8 as follows [11]:

$$l_e \approx 2(h_w + b_w + 2.5b_c), A_c = 2b_c w_t \quad (6)$$

From (6), the magnetizing inductance can be calculated from the physical dimensions of the ferrite core and the winding turns as follows:

$$L_m = \frac{\mu_0 \mu_r N_p^2 A_c}{l_e} \quad (7a)$$

$$\therefore L_p = L_m + L_{l,p} \approx L_m \quad (L_m \gg L_{l,p}) \quad (7b)$$

The winding arrangement of the proposed transformers is shown in Fig. 9, assuming that four winding layers for primary and secondary windings are positioned within the window area. There are multiple winding layers having winding turns, and primary windings are in the center position w.r.t. the  $z$ -axis. The total primary and secondary winding turns can then be expressed as follows:

$$N_p = \sum_{j=1}^{m_p} n_{p,j}, N_s = \sum_{j=1}^{m_s} n_{s,j}, \text{ for } (j = 1, 2, \dots, m_p \text{ or } m_s) \quad (8)$$

The leakage calculation process presented in this section is based on the magnetic field distribution in the transformer and this calculation method is applied to the proposed transformer winding structure to find the equivalent leakage inductance [20]. It is noteworthy that all the magnetizing magnetic components pass through the ferrite core, whereas leakage magnetic components only exist in the window area; an arbitrary magnetic field distribution in the window area hence should be specified. The magnetic field strength w.r.t.  $z$ -axis distance  $H(z)$  for arbitrary ampere-turn winding can then be defined as follows [20]:

$$\oint H dA = \frac{NI}{h} z \rightarrow H(z) = \frac{NI}{b_w h} z \quad [A/m] \quad (9)$$

where  $h$  is the thickness of the copper winding, as shown in Fig. 9, where  $h_p$  and  $h_s$  are the thickness of the primary and secondary windings, respectively, and  $h_{po}$  and  $h_{so}$  are the gap between each winding turns.  $h_d$  is the gap between primary and secondary winding.

Based on the theoretical derivations of (8)–(9), the magnetic field strength distribution  $H(z)$ , which is proportional to the magneto-motive-force ( $mmf$ ), can be calculated, as shown in Fig. 9. In the case of primary ampere-turn winding, if  $z$  is within the ampere-turn position,  $H(z)$  can be expressed as follows:

$$H(z) = \frac{I_p}{b_w} \left[ \sum_{k=1}^{j-1} n_{p,k} + \frac{n_{p,j}}{h_p} \{z - (j-1)(h_p + h_{po})\} \right]$$

$$\text{for } (j-1)(h_p + h_{po}) \leq z < j(h_p + h_{po}) - h_{po} \quad (10)$$

By the same principle,  $H(z)$  can be calculated for gap positions  $h_{po}$  and  $h_d$  as follows:

$$H(z) = \frac{I_p}{b_w} \sum_{k=1}^j n_{p,k} \text{ for } j(h_p + h_{po}) - h_{po} \leq z < j(h_p + h_{po}) \quad (11a)$$

$$H(z) = \frac{I_p}{b_w} \sum_{k=1}^{0.5m_p} n_{p,k} \text{ for } m_p h_p + (m_p - 1) h_{po} \leq z \\ < m_p h_p + (m_p - 1) h_{po} + h_d. \quad (11b)$$

By the same theoretical approach of (10)–(11), the secondary ampere-turn cases can be also found.

Based on (10)–(11), the total energy stored by leakage magnetic flux within the window area  $E_t$  can be derived as follows:

$$E_t = \frac{1}{2} \int_V B \cdot H dV = \frac{\mu_0 b_w l_m}{2} \cdot \int_0^{h_w} H^2(z) dz = \frac{1}{2} \sum_{i=s,p} L_{l,i} \cdot I_i^2 \quad (12)$$

where  $l_m$  is the mean length in each winding turn. It is noted from (12) that leakage inductance for primary and secondary sides  $L_{l,p}$  and  $L_{l,s}$  is a function of  $H(z)$ .

For simplicity of analysis, if  $h_{po} = h_{so} = h_d \equiv h_n$  and  $m_p = m_s = m_n$ , the total leakage energy can be further simplified as follows:

$$E_t = \frac{\mu_0 l_m}{b_w} \sum_{i=s,p} \left[ I_i^2 \sum_{j=1}^{0.5m_n} \left\{ \frac{1}{2} (h_i + h_n) (n_{i,j}^2 + n_{i,j+1}^2) \right. \right. \\ \left. \left. + n_{i,j}^2 (h_i + h_n) \right\} \right] \quad (13)$$

where the primary and secondary ampere-turns are assumed to be the same, i.e.,  $N_p I_p = N_s I_s$  in (13).

From (10)–(13), equivalent leakage inductance  $L_{l,p}$  and  $L_{l,s}$  can be found under the given physical dimensions and ampere-turns by proposed numerical methodology.

### C. Transformer Loss

Transformer loss is mainly composed of core loss and copper loss [11]–[14]. There are several methods to estimate the core loss for high-frequency transformers [21]–[24]. In the case of sinusoidal waveforms of the primary and secondary currents with phase difference information, the original Steinmetz equation is the simplest and most popular method [21]. In the case of non-sinusoidal waveforms for DAB converters, as identified from Fig. 7, the change rate of the magnetic field  $dB_c/dt$ , which is proportional to the magnetizing current  $I_m$  in (3)–(4), needs to be considered in the time domain. For this reason, the improved generalized Steinmetz equation (IGSE) to reflect the DAB current waveforms can be used as follows [22]–[23]:

$$P_{cv} = \frac{1}{T_s} \int_0^{T_s} k_c \left| \frac{dB_c(t)}{dt} \right|^\alpha (\Delta B_c)^{\beta-\alpha} dt \quad [\text{kW/cm}^3] \quad (14a)$$

$$\therefore k_c = \frac{C_m}{(2\pi)^{\alpha-1} \int_0^{2\pi} |\cos \theta|^\alpha 2^{\beta-\alpha} d\theta} \quad (14b)$$

where  $C_m$ ,  $\alpha$ , and  $\beta$  are the major parameters determined by magnetic characteristics [21]–[23]. According to the datasheet of the ferrite core used in this paper, i.e., PM12 in the datasheet, the values of  $C_m$ ,  $\alpha$ , and  $\beta$  can be obtained by a dataset of power loss, operating frequency, and magnetic flux density, as follows [25]:  $C_m = 6.40$ ,  $\alpha = 1.31$ , and  $\beta = 2.62$ .

Then, the core loss can be analytically calculated from (14) as follows:

$$P_{co} = \iiint P_{cv} dx dy dz \approx P_{cv} U_c \quad (15)$$

where  $U_c$  is the total volume of the proposed integrated transformer core part.

On the other hands, the copper loss can be simply calculated by current and AC winding resistance as follows:

$$P_{cp} = I_p^2 r_{c,p} + I_s^2 r_{c,s} \quad (16)$$

where  $I_p$  and  $I_s$  can be calculated from (1b), and  $r_{c,p}$  and  $r_{c,s}$  in Fig. 6 can be obtained by calculation or simulation if the geometrical information of the copper winding and switching frequency is given [11], [23]–[24].

From (15)–(16), the transformer loss  $P_{ct}$  is the summation of  $P_{co}$  and  $P_{cp}$ , and will be evaluated by simulation verification.

### D. HV Insulation Design

Considering 170 A and 220 A for the primary and secondary currents  $I_p$  and  $I_s$ , as identified from Fig. 4, 133 mm<sup>2</sup> and 157 mm<sup>2</sup> Litz copper wires are selected for primary and secondary windings, respectively, throughout this paper [26]–[27]. Then, to satisfy the HV insulation requirements, i.e., 60 kV in this paper, HV insulation capability is necessary for copper wires. To meet the insulation requirement between the HV and LV stacks, the proposed transformers should guarantee at least 60 kV insulation capability for two cases: 1) between the primary coil and secondary coil and 2) between the primary coil and ferrite core. As the first insulation material nearest to the Litz copper wire, 1.0 T Kapton polyimide film tape is used not only to add insulation capability but also to appropriately fix

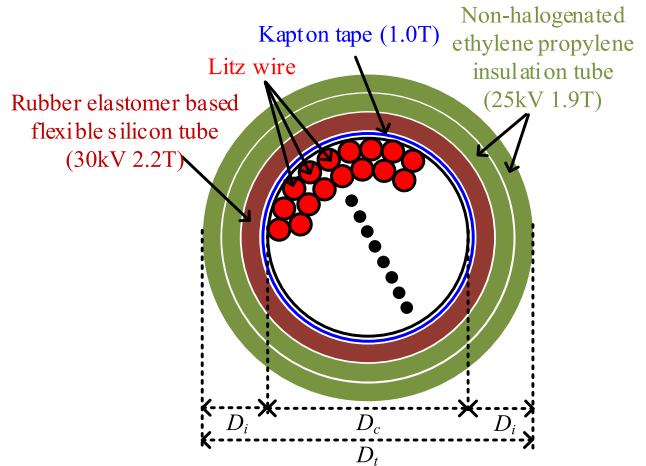


Fig. 10. HV insulation structure for the copper winding.

TABLE II  
COPPER WINDING SELECTION FOR HV INSULATION

Primary winding [mm]			Secondary winding [mm]		
$D_c$	$D_i$	$D_t$	$D_c$	$D_i$	$D_t$
13	7	27	15	7	29

the form of Litz copper wire for insulation manufacture, as shown in Fig. 10. The second insulation material is a rubber elastomer based flexible silicon tube, which can withstand 30 kV at 2.2T. The third insulation material is a non-halogenated ethylene propylene insulation tube (25 kV at 1.9 T) and two tubes are used for 50 kV at 3.8 T. The first and second insulation layers have a flexible feature for easily bending the copper wires; however, they are relatively expensive. On the other hand, the third insulation layer is inexpensive and easily manufactured, but is rather stiff. From this proposed insulation structure, at least 80 kV insulation capability can be possible for an ideal case. The physical dimensions of the copper windings are summarized in Table II. Therefore, by combining these proposed insulation layers, easy assembly and economical manufacture with HV insulation capability are possible.

### IV. DESIGN RESULTS AND SIMULATION VERIFICATIONS

To appropriately design the proposed transformer and evaluate the major characteristics, several combinations for primary and secondary winding turns have been selected, as shown in Fig. 11. When  $N_p$  changes,  $N_s$  is appropriately selected for  $1.3 \leq n_a \leq 1.5$  in Table I. Because the ferrite core is on the LV side, the secondary winding and the ferrite core can be adjacent, whereas the primary windings are surrounded by epoxy molding for HV insulation. Based on the simulation model of Fig. 11, the equivalent leakage inductance is calculated from (9)–(13) and compared with 3D finite-element-method (FEM) simulation results, as shown in Fig. 12, where the calculation and simulation results are matched well with each other. Although the exact value of 35.0  $\mu$ H cannot be found due to the integer value of winding turns, the nearest value of 33.5  $\mu$ H is selected:  $N_p = 8$

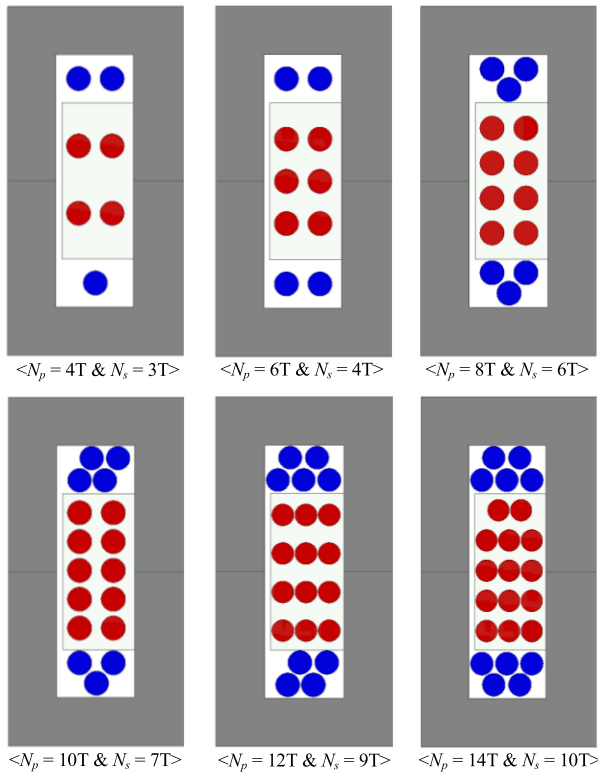


Fig. 11. Copper winding arrangement for  $4T \leq N_p \leq 14T$ .

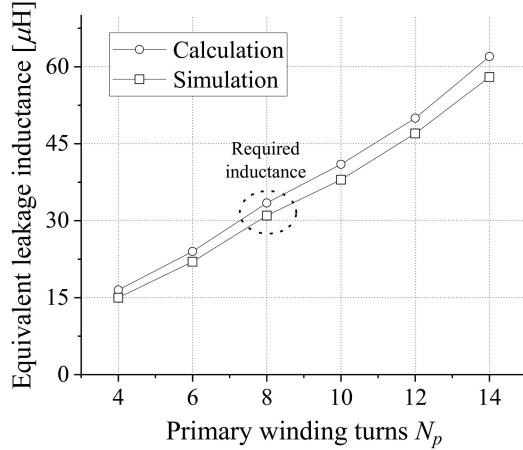


Fig. 12. Calculation and simulation results of leakage inductance.

turns and  $N_s = 6$  turns in this paper. When appropriate values of  $N_p$  and  $N_s$  are determined, the magnetic field inside the ferrite core  $B_c$  should be confirmed, regarding whether  $B_c < 0.3$  T, as shown in Fig. 13. The core can be saturated when  $N_p < 5$  T, whereas  $B_c = 0.16$  T for  $N_p = 8$  turns, which are appropriate results in terms of the core saturation level. Based on (9)–(11), the magnetic field strength is calculated and compared with the simulation results, as shown in Fig. 14, where the calculation results are in good agreement with simulation results.

In order to specify the loss characteristics w.r.t. the secondary winding position, two 3D simulation model is built, as shown in Fig. 15. As an intuitive design example, primary and secondary

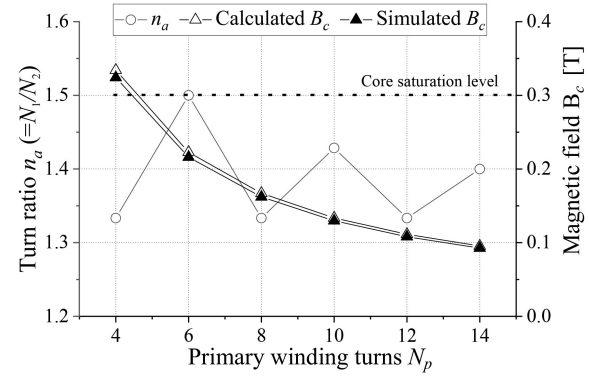


Fig. 13. Selected turn ratio and magnetic field inside the core.

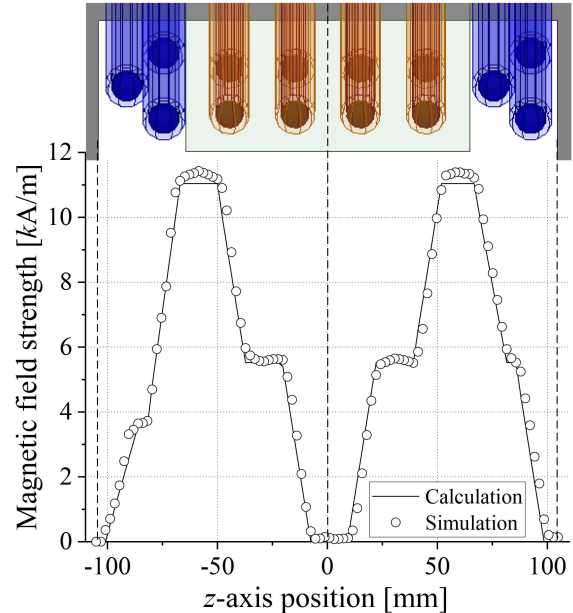


Fig. 14. Calculation and simulation results of the magnetic field strength w.r.t. z-axis position.

windings can be stacked in series, as shown in Fig. 15(a). Although the winding structure in Fig. 15(a) is the most popular, primary and secondary magnetic fields may not be completely canceled out inside the ferrite core. To effectively cancel out the primary magnetic field inside the ferrite core by the secondary magnetic field, secondary windings are separated to upper and lower sides, as shown in Fig. 15(b). In order to verify the difference between the conventional and proposed transformer structures in Fig. 15, the simulation results under maximum operating conditions are shown in Fig. 16. As a result, the core losses for the conventional and proposed transformer structures are 103.0 W and 95.1 W, respectively; hence, 7.7% core loss improvement can be obtained by the proposed two-separated secondary winding structure.

From the theoretical analysis and 3D simulation model, the core and copper losses are investigated, as shown in Fig. 17. When  $N_p$  increases, the core loss decreases, whereas the copper loss increases. Therefore, the optimal  $N_p$  exists for minimum transformer loss:  $N_p = 8$  turns and  $N_s = 6$  turns are an optimal

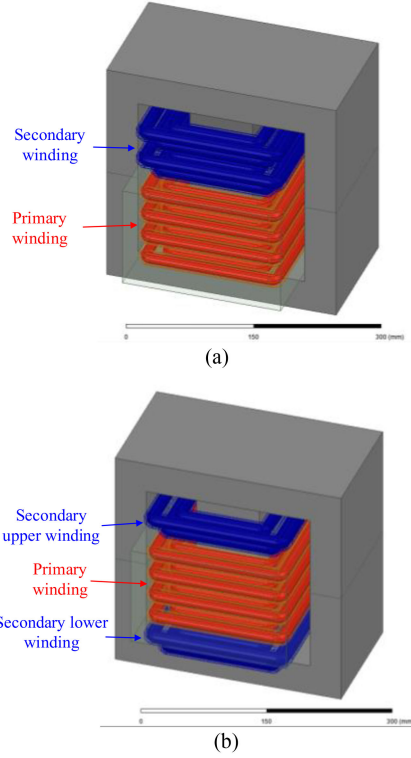


Fig. 15. 3D simulation model of the conventional and proposed integrated transformers. (a) Conventional winding structure. (b) Proposed winding structure.

design point. According to the results of Fig. 17,  $P_{co} = 95.1$  W and  $P_{cp} = 260.0$  W; the transformer loss  $P_{ct}$  is hence 355.4 W.

Based on the theoretical and simulation results in this section, the temperature characteristics at the steady state are investigated for the proposed transformers, as shown in Fig. 18. Although the transformers may be exposed to driving wind in railway vehicles, it is assumed in this 3D simulation that there is no driving wind and heat dissipation is radiating everywhere under an ambient surrounding temperature of 25°C. According to the simulation results, as shown in Fig. 18, the maximum temperature points of the ferrite core and copper wire are 116.6°C and 95.2°C, respectively.

In order to confirm the HV insulation capability, the simulation winding model is built, according to Fig. 10 and Table II. In the 3D simulation conditions, 60 kV voltage is applied to the primary winding and zero voltage is applied to the secondary winding and the ferrite core. As a result, all the electrical field are below 2 kV/mm, corresponding with the most severe dielectric breakdown value, as shown in Fig. 19. Because for this 3D simulation result it is assumed that all the components are ideal, experimental confirmation is mandatory by a real-scaled prototype, which will be performed in the experimental verification. All the electrical and magnetic characteristics have been specified in this section, and the detailed design procedures are summarized in Fig. 20. The increments of the temperature rise for the core and copper  $\Delta T_{co}$  and  $\Delta T_{cp}$  are assumed to be below 110°C, considering the melting temperature of the copper wire insulation, in this paper. If the electrical field standard ( $<20$

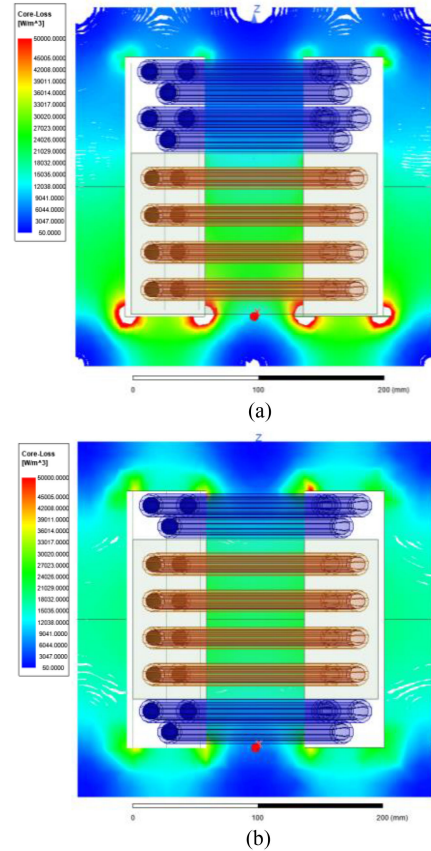


Fig. 16. Simulation results of the conventional and proposed integrated transformers. (a) Conventional one. (b) Proposed one.

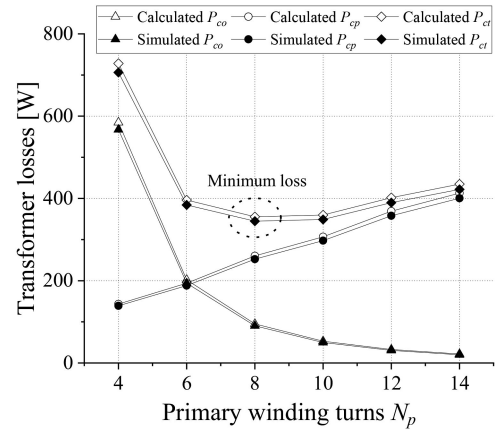
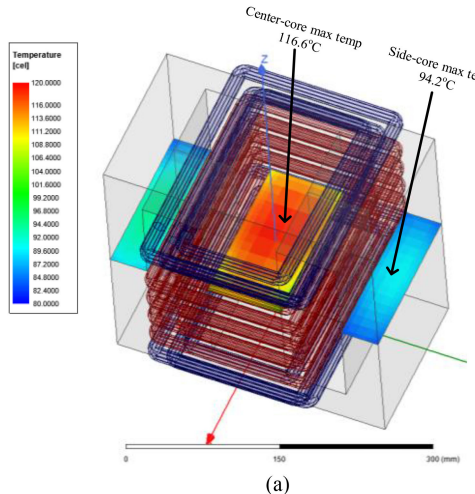
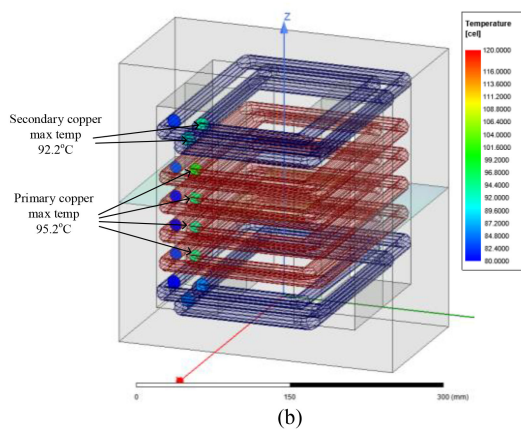


Fig. 17. Calculation and simulation results of the transformer loss w.r.t.  $N_p$ .

kV/mm) is not satisfied,  $D_i$  should be increased for improved HV insulation; hence, the total copper area for the primary and secondary windings  $A_p$  and  $A_s$  should be resized again. If all the temperatures and HV insulation characteristics satisfy with the proposed design criteria, it can be stated that the proposed integrated transformers are suitable for the SST applications. By virtue of the proposed design process in Fig. 20, highly efficient and high voltage insulation transformer can be designed,



(a)



(b)

Fig. 18. The temperature characteristics of the proposed integrated transformers by 3D FEM simulation analysis. (a) Core temperature. (b) Copper winding temperature.

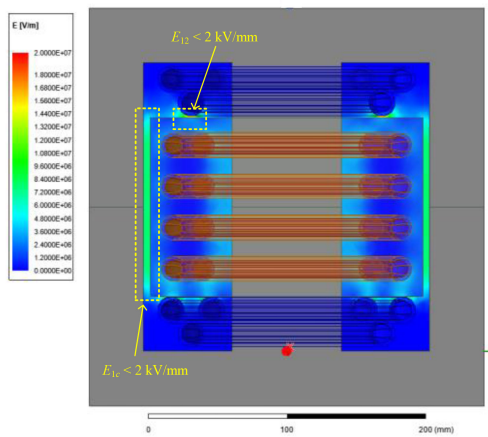


Fig. 19. The E-field electrical characteristics of the proposed transformers by 3D FEM simulation analysis.

although the installation space for the transformer in SST is already given.

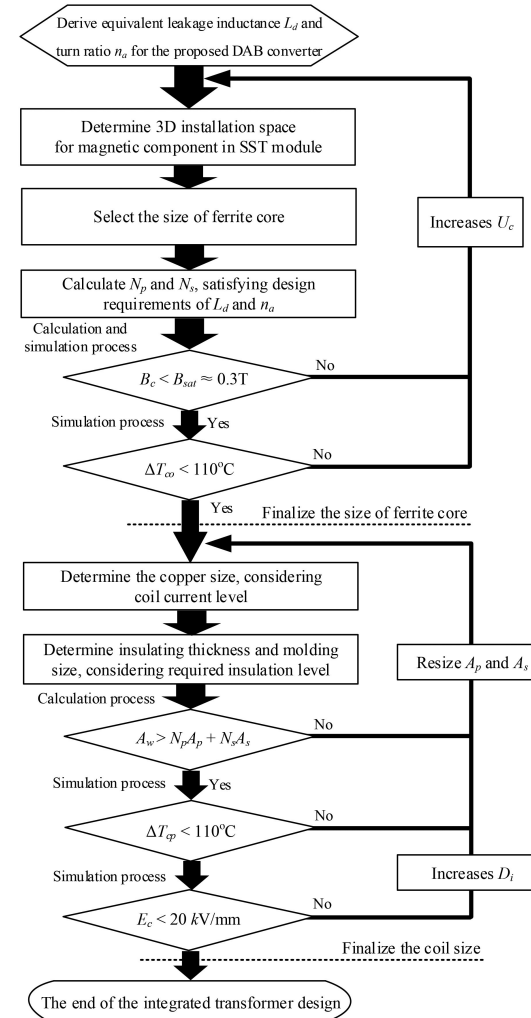


Fig. 20. The design flow chart for the proposed transformers.

## V. EXPERIMENTAL VERIFICATION

### A. Fabrications and Measurement of the Conventional and Proposed Transformers for the SST

To evaluate the proposed integrated transformers and to compare the proposed and the conventional transformers, the proposed transformer sets were fabricated in accordance with the proposed design procedure in Fig. 20, as shown in Fig. 21(a)–(b). On the other hand, the conventional transformer set including isolation transformers and additional inductors in Fig. 21(c) was fabricated based on the previous transformer design procedure, satisfying 250 kW design requirements for high efficiency operation of DAB converters [1]. The total size of the conventional transformer set is 320 mm × 300 mm × 650 mm, whereas that of the proposed set is 320 mm × 300 mm × 620 mm; both transformer sets hence can be installed within the allowable installation space for the proposed SST, as identified from Fig. 3, and the proposed set is 4.7% smaller than the conventional set. The measured total weights for the conventional and proposed transformer sets are 116.0 kg and 107.9 kg, respectively; hence,

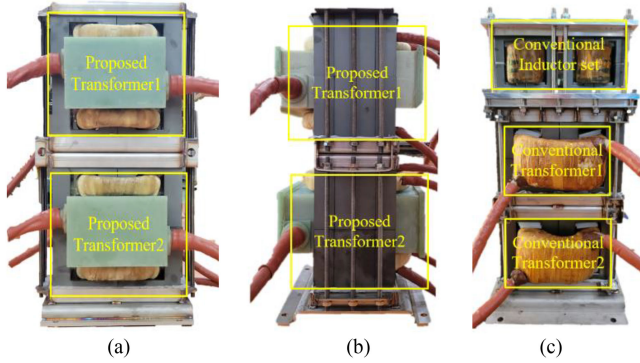


Fig. 21. Prototypes of the conventional and proposed transformers. (a) Proposed one (Front view). (b) Proposed one (Side view). (c) Conventional one (Front view).

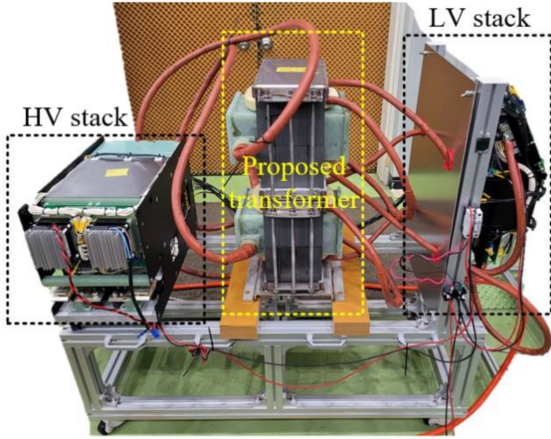


Fig. 22. The fabricated 250 kW SST module.

7.0% weight reduction can be obtained by removing the additional inductors. Notably, the length and width of the conventional and proposed transformers are the same at 320 mm × 300 mm, whereas the height of the proposed integrated transformers is greater than that of the only conventional transformer without additional inductors. This height increment of the transformers is implemented to enhance the HV insulation capability between the primary and secondary windings, and to increase both the heat dissipation capability and the inherent leakage inductance.

The proposed integrated transformer set is installed between HV and LV stacks, as shown in Fig. 22. In the HV stack, the HV-insulation-based IGBT gate-driver-units (GDU) are used for AC/DC converters, and the gate signals are provided from the module controller in the LV stack by optic cables. To drive 2.3 kV HV voltage for one SST module, 6.5 kV / 400 A FZ400R65KE3 IGBT switching devices made by Infineon are used for the AC/DC converters. Because the module DC link voltage  $V_{dc}$  is regulated to be 4.0 kV, 3.3 kV / 750 A FMF750DC-66A SiC power switching devices made by Mitsubishi are used for the primary DAB converters. Thus, a 6.6 kV voltage rating is possible due to two series connections for the DAB converters, and its voltage stress margin is calculated as 65.0%. In the LV stack, TMS320F28377 DSP is used for the module controller,

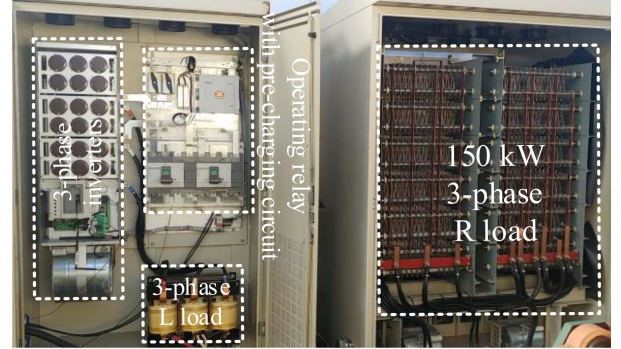


Fig. 23. 125 kW active load having 3 phase R-L loads.

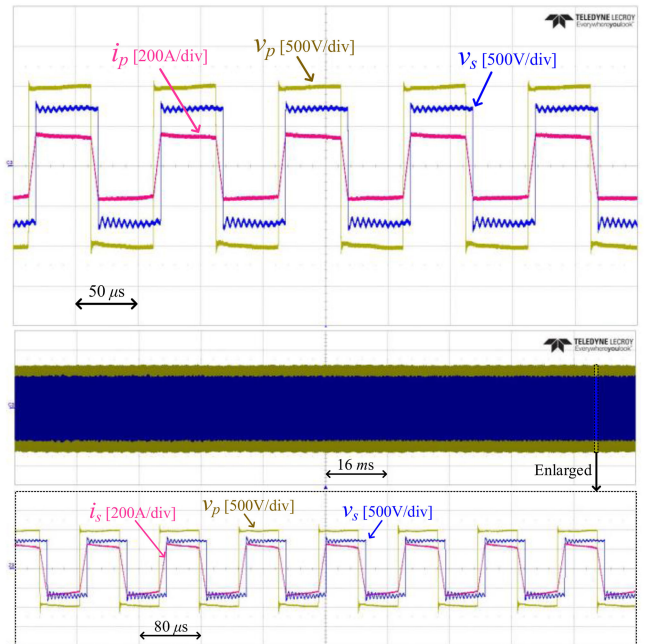


Fig. 24. Voltage and current waveforms of the proposed integrated transformers.

and all the gate and fault signals are connected from this module controller. For the secondary DAB converters, 1.2 kV / 800 A FMF800DX-24B SiC power switching devices made by Mitsubishi are used. Thus, a 2.4 kV voltage rating is possible in the 1.5 kV load side due to the use of two series connections for the DAB converters, and the voltage stress margin is calculated as 60.0%. A continuous active load to verify one DAB converter for 125 kW rated load condition was manufactured, as shown in Fig. 23. The active load in Fig. 23 is based on three-phase inverters having three-phase RL loads. The input and the output of this active load inverter are DC 750 V and AC three-phase resistance (R) & inductance (L) loads, respectively. The voltage and current waveforms of the proposed integrated transformers are shown in Fig. 23, and they are consistent with the simulation results in Fig. 4. To verify the proposed numerical design methodology to obtain the appropriate leakage inductance, equivalent leakage inductance is measured, as shown in Fig. 25. The total leakage inductance has been measured from the secondary side by shorting the primary windings. In this case, it is assumed that

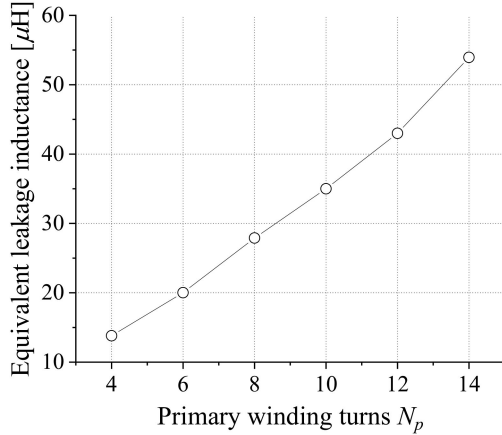


Fig. 25. Measured results of the equivalent leakage inductance.

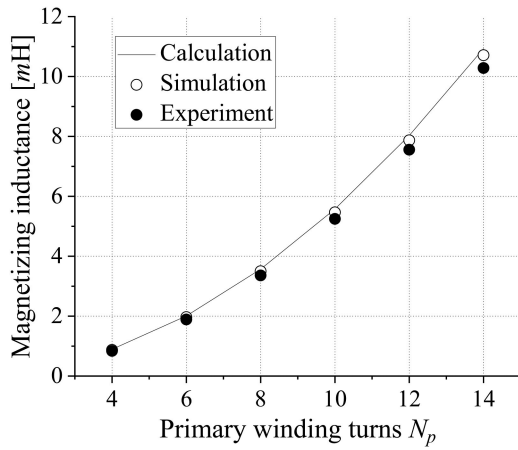
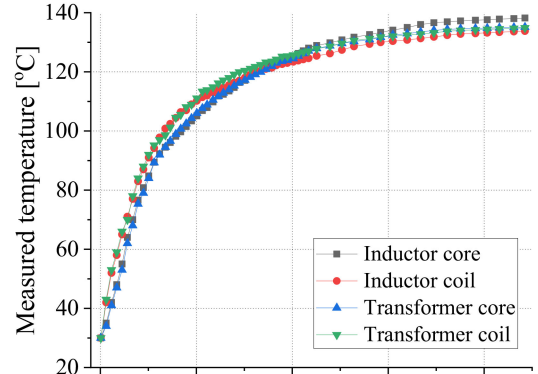


Fig. 26. Measured results of the magnetizing inductance.

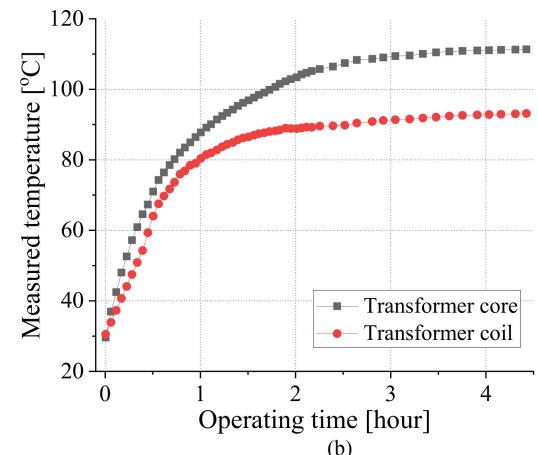
the magnetizing inductance is extremely larger than the leakage inductance. Nevertheless, the measured results in Fig. 25 are in good agreement with the calculation and simulation results of Fig. 12. The magnetizing inductance was also measured w.r.t.  $N_p$ , as shown in Fig. 26, and the results are in good agreement with the calculation and simulation results.

### B. Temperature Characteristics

As identified from Fig. 18, the thermally stable operation is an important factor if the equivalent leakage inductance meets the design requirements. Based on the optimally designed conventional and proposed transformers, the major measured points are selected, and their temperatures are measured during 4.5 hours of operation, as shown in Fig. 27, where a Graphtec GL840 measurement device is used in this paper. It is assumed that 125 kW active load operates and there is no external wind in the experimental environment. After 4.5 hours, the measured temperatures are almost saturated for both the conventional and proposed transformers: the maximum temperatures for the conventional inductors and transformers were measured as 138.2°C and 135.1°C, respectively. In case of the proposed transformer, the saturated temperatures for the core and copper are 111.3°C and 93.1°C, respectively, which are in good agreement with



(a)



(b)

Fig. 27. Temperature measurement results of the transformers. (a) Conventional transformer sets. (b) Proposed transformer sets.

the simulation results of Fig. 18. Because these transformers would operate for a long period of time for railway vehicle SST applications, the final saturation temperatures should be investigated based on the measured temperatures and the results are shown in Fig. 28. As a result, the expected final temperatures for the conventional and proposed transformers are 138.7°C and 112.8°C, respectively. Therefore, the proposed transformer provides 25.9°C temperature improvement compared to the conventional transformer. Considering the fact that the ambient temperature is 28.8°C in the surrounding experimental environment temperature, i.e., ambient temperature, the maximum temperature increment of the proposed transformer for core and copper  $\Delta T_{co,max}$  and  $\Delta T_{cp,max}$  are calculated as 82.5 and 64.3, respectively. These increment values are highly less than the critical values of 110.0 in Fig. 20. Therefore, although the proposed transformer operates under the severe hot environment, e.g., 40.0°C ambient temperature, it would be safe because the maximum temperature of the transformer is still well below a melting temperature of the copper winding with insulation material in the transformers.

Maximum temperature points are captured by a thermal camera after 4.5 hours of operation, as shown in Fig. 29. The highest temperature points for the conventional transformer are

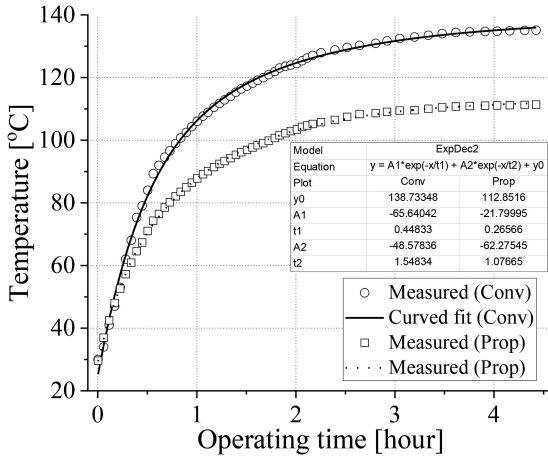


Fig. 28. Curve-fitting results of the steady-state temperature based on the measured results.

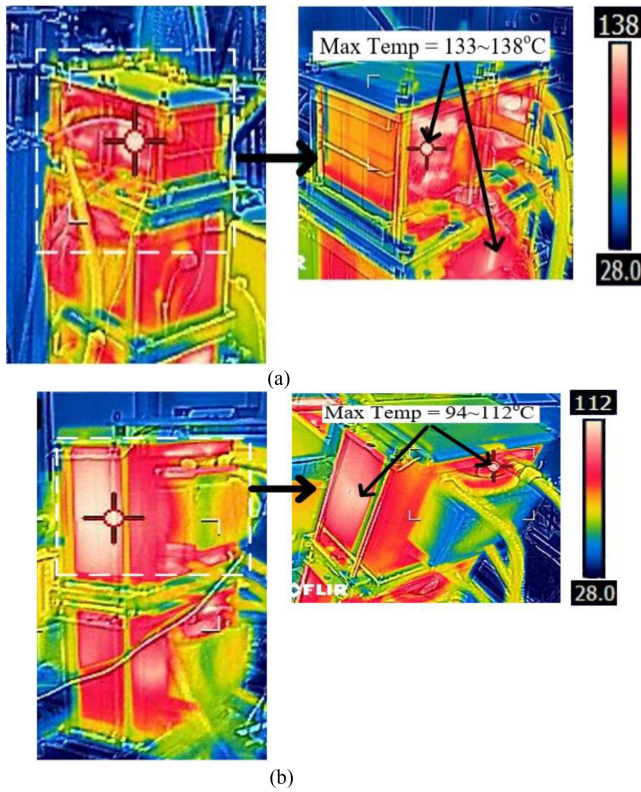


Fig. 29. Maximum temperature measurement points after 4.5 hours. (a) Conventional transformer sets. (b) Proposed transformer sets.

the inductor core and transformer core, as shown Fig. 29(a), where 138°C temperature points have been observed. On the other hands, the maximum temperature point for the proposed transformer is the center-core, which is the most severe point for heat dissipation, as shown in Fig. 29(b). Because the expected value of the final temperature is 112.8°C, this temperature level is highly improved compared to the conventional transformer and sufficiently stable to sustain long time operation of the proposed SST. The transformer efficiency was measured as

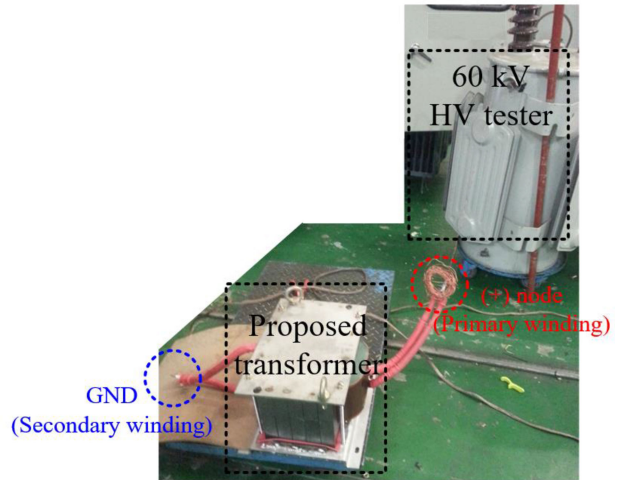


Fig. 30. The test environment for HV insulation of the proposed integrated transformer.

99.7%; this result is similar with the simulation results of Fig. 17 and has been obtained by a precise measurement device, i.e., DEWETRON 2600 in this paper.

### C. HV Insulation Capability

After ensuring the temperature characteristics satisfy with the temperature standard for thermally stable operation, the HV insulation characteristics should be specified in order to verify the simulation results of Fig. 19. To experimentally verify the HV insulation capability of the conventional and proposed transformers, a voltage-variable HV test environment was built, as shown in Fig. 30. Two primary winding nodes are tied and connected to the (+) node. In the same manner, two secondary winding nodes and the body of the ferrite core are tied together and connected to ground. As a result, although the conventional transformer in Fig. 21(c) experiences dielectric breakdown at 45 kV voltage, the proposed transformer in Fig. 21(a)–(b) operated until 60 kV by virtue of the HV insulation design in Fig. 10.

## VI. CONCLUSION

In this paper, a high-efficiency and HV insulation integrated transformer, having inherent leakage inductance, has been introduced and verified by simulation and experiments for railway vehicle SST applications. Although the railway vehicle has a severe constraint for the installation space of the proposed SST, the high-frequency transformers in the DC/DC converters can be appropriately manufactured and installed according to the proposed transformer design procedure. In order to design the required equivalent leakage inductance and to minimize the transformer loss under given physical dimension of the transformers, the number of winding turns can be appropriately selected. Furthermore, a practical copper wire structure is proposed for cost-effective, thermal-stable operation and 60 kV HV insulation capability. Finally, 125 kW conventional and proposed transformers have been manufactured and comparatively evaluated by a 250 kW SST module, and the results show

that the proposed transformers are superior to the conventional transformers in all aspects, i.e., size, weight, temperature, and HV insulation.

## REFERENCES

- [1] E. S. Lee, J. H. Park, M. Y. Kim, and J. S. Lee, "High efficiency module design of solid-state transformers for railway vehicles," *IEEE Trans. Transp. Electrific.*, vol. 8, no. 1, pp. 98–120, Mar. 2022.
- [2] J. Feng, W. Q. Chu, Z. Zhang, and Z. Q. Zhu, "Power electronic transformer-based railway traction systems: Challenges and opportunities," *IEEE J. Emerg. Sel. Topics Power Electron.*, vol. 5, no. 3, pp. 1237–1253, Sep. 2017.
- [3] A. Iraklis, T. Schirmer, H. Dittus, A. Lusiewicz, and J. Winter, "Overview of three-stage power converter topologies for medium frequency-based railway vehicle traction systems," *IEEE Trans. Veh. Tech.*, vol. 68, no. 4, pp. 3268–3278, Apr. 2019.
- [4] M. A. Hannan *et al.*, "State of the art of solid-state transformers: Advanced topologies, implementation issues, recent progress and improvements," *IEEE Access*, vol. 8, pp. 19113–19132, Jan. 2020.
- [5] J. Zhang, J. Liu, S. Zhong, J. Yang, N. Zhao, and T. Q. Zheng, "A power electronic traction transformer configuration with low-voltage IGBTs for onboard traction application," *IEEE Trans. Power Electron.*, vol. 34, no. 9, pp. 8453–8467, Sep. 2019.
- [6] L. Zheng, R. P. Kandula, and D. Divan, "Current-source solid-state DC transformer integrating LVDC microgrid, energy storage and renewable energy into MVDC grid," *IEEE Trans. Power Electron.*, vol. 37, no. 1, pp. 1044–1058, Jan. 2022.
- [7] C. A. d. Santos, L. C. d. S. Mazza, F. L. Tofoli, D. d. S. Oliveira Junior, P. P. Praça, and F. L. M. Antunes, "Four-port, single-stage, multi-directional AC-AC converter for solid-state transformer applications," *IEEE Trans. Ind. Electron.*, vol. 69, no. 5, pp. 4596–4606, May 2022.
- [8] Y. Sun, Z. Gao, C. Fu, C. Wu, and Z. Chen, "A hybrid modular DC solid-state transformer combining high efficiency and control flexibility," *IEEE Trans. Power Electron.*, vol. 35, no. 4, pp. 3434–3449, Apr. 2020.
- [9] N. Hou and Y. Li, "Overview and comparison of modulation and control strategies for nonresonant single-phase dual-active-bridge dc-dc converter," *IEEE Trans. Power Electron.*, vol. 35, no. 3, pp. 3148–3172, Mar. 2020.
- [10] D. Das, N. Weise, K. Basu, R. Baranwal, and N. Mohan, "A bidirectional soft-switched DAB-based single-stage three-phase AC-DC converter for V2G application," *IEEE Trans. Transp. Electrific.*, vol. 5, no. 1, pp. 186–199, Mar. 2019.
- [11] E. S. Lee, J. H. Park, M. Y. Kim, and S. H. Han, "An integrated transformer design with a center-core air-gap for DAB converters," *IEEE Access*, vol. 9, pp. 121263–121278, Aug. 2021.
- [12] M. Mu, L. Xue, D. Boroyevich, B. Hughes, and P. Mattavelli, "Design of integrated transformer and inductor for high frequency dual active bridge GaN charger for PHEV," in *Proc. IEEE Appl. Power Electron. Conf. Expo.*, 2015, pp. 579–585.
- [13] B. Cougo and J. W. Kolar, "Integration of leakage inductance in tape wound core transformers for dual active bridge converters," in *Proc. 7th Int. Conf. Integr. Power Electron. Syst.*, Nuremberg, Germany, 2012, pp. 1–6.
- [14] B. Sun, R. Burgos, and D. Boroyevich, "Modeling and optimization of high-frequency litz-wire transformer for 10 kW gan-based LLC resonant converter," in *Proc. IEEE 19th Workshop Control Model. Power Electron. (COMPEL)*, 2018, pp. 1–7.
- [15] Y. Liu, H. G. Wu, J. Zou, Y. Tai, and Z. Ge, "CLL resonant converter with secondary side resonant inductor and integrated magnetics," *IEEE Trans. Power Electron.*, vol. 36, no. 10, pp. 11316–11325, Oct. 2021.
- [16] M. H. Ahmed, A. Nabih, F. C. Lee, and Q. Li, "Low-loss integrated inductor and transformer structure and application in regulated LLC converter for 48-V bus converter," *IEEE J. Emerg. Sel. Topics Power Electron.*, vol. 8, no. 1, pp. 589–600, Mar. 2020.
- [17] Z. Ouyang, W. G. Hurley, and M. A. E. Andersen, "Improved analysis and modeling of leakage inductance for planar transformers," *IEEE J. Emerg. Sel. Topics Power Electron.*, vol. 7, no. 4, pp. 2225–2231, Dec. 2019.
- [18] J. Zhang, Z. Ouyang, M. C. Duffy, M. A. E. Andersen, and W. G. Hurley, "Leakage inductance calculation for planar transformers with a magnetic shunt," *IEEE Trans. Ind. Appl.*, vol. 50, no. 6, pp. 4107–4112, Nov. 2014.
- [19] Y. Liu, X. Huang, Y. Dou, Z. Ouyang, and M. A. E. Andersen, "GaN-based ZVS bridgeless dual-SEPIC PFC rectifier with integrated inductors," *IEEE Trans. Power Electron.*, vol. 36, no. 10, pp. 11483–11498, Oct. 2021.
- [20] E. C. Snelling, *Soft Ferrites, Properties and Applications*, 2nd ed. London, Butterworth-Heinemann, 1988.
- [21] C. P. Steinmetz, "On the law of hysteresis," *Proc. IEEE*, vol. 72, no. 2, pp. 197–221, Feb. 1984.
- [22] I. Villar, U. Viscarret, I. Etxeberria-Otadui, and A. Rufer, "Global loss evaluation methods for nonsinusoidally fed medium-frequency power transformers," *IEEE Trans. Ind. Electron.*, vol. 56, no. 10, pp. 4132–4140, Oct. 2009.
- [23] P. Huang *et al.*, "Optimal design and implementation of high-voltage high-power silicon steel core medium-frequency transformer," *IEEE Trans. Ind. Electron.*, vol. 64, no. 6, pp. 4391–4401, Jun. 2017.
- [24] J. Ferreira, "Appropriate modelling of conductive losses in the design of magnetic components," in *Proc. 21st Annu. IEEE Conf. Power Electron. Specialists*, 1990, pp. 780–785.
- [25] Toda-isu, *Ferrite core datasheet*. [Online]. Available: <http://forum.cxem.net/applications/core/interface/file/attachment.php?id=318271>
- [26] *Electric cables - calculation of the current rating, part 1: current rating equations (100% load factor) and calculation of losses, section 1: General*, IEC 60287-1-1, 2006.
- [27] NFPA 70: National Electrical Code, 1st ed., *National Fire Protection Association (NFPA)*, 2017.



**Eun S. Lee** (Member, IEEE) received the B.S. degree in electrical engineering from Inha University, Incheon, South Korea, in 2012, and the M.S. and Ph.D. degrees in nuclear and quantum engineering from the Korea Advanced Institute of Science and Technology, Daejeon, South Korea, in 2014 and 2017, respectively. From 2017 to 2019, he was with LG Electronics CTO Power Electronics Lab, Seoul, South Korea. From 2019 to 2022, he was a Senior Researcher with Propulsion System Research Team, Korea Railroad Research Institute, Uiwang, South Korea. Since 2022, he has been with Hanyang University ERICA Campus, where he is currently an Assistant Professor with the School of Electrical Engineering. His research interests include power converters, multilevel converters, and wireless power transfer systems.



**Jin H. Park** (Member, IEEE) received the B.S. and Ph.D. degrees in electronic engineering from Ajou University, Suwon, South Korea, in 2013 and 2018, respectively. Since 2018, he has been with Smart Electrical & Signaling Division Propulsion Research Team, Korea Railroad Research Institute, Uiwang, South Korea. His research interests include power conversion and grid-connected systems.



**Myung Y. Kim** (Member, IEEE) received the B.S. and M.S. degrees in electrical engineering from Chung-Ang University, Seoul, South Korea, in 1989 and 1991, respectively. From 1991 to 1995, he was a Senior Researcher with the Traction Research Group of Hyundai Precision & Industries Company, Seoul, South Korea, where he developed propulsion systems for urban-railway vehicles. Since 1995, he has been a Senior and Principal Researcher with Korea Railroad Research Institute, Uiwang, South Korea. His research interests include wireless power transfer systems and power converter systems especially for railway vehicles.



**June S. Lee** (Member, IEEE) received the B.S., M.S., and Ph.D. degrees in electrical and computer engineering from Ajou University, Suwon, South Korea, in 2011, 2013, and 2015, respectively. From 2015 to 2020, he was a Senior Researcher with the Propulsion System Research Team of the Korea Railroad Research Institute, Uiwang, South Korea. In 2020, he joined the School of Electronics and Electrical Engineering, Dankook University, Yongin, South Korea. His research interests include high power electric machine drives, grid-connected systems, multilevel inverter, and reliability.